Integrated Parallel Beam WDS/EDS Analysis: Benefits and Limitations for Geoscience Research

Giancarlo Capitani, Roberto Conconi, Niccolò Magnani, Stefano Zanchetta, Michael Abratis

Microscopy and Microanalysis, 2025, **31**, ozaf101
https://doi.org/10.1093/mam/ozaf101
Advance access publication 27 October 2025
Original Article

Microscopy AND Microanalysis

Integrated Parallel Beam WDS/EDS Analysis: Benefits and Limitations for Geoscience Research

Giancarlo Capitani[1,*], Roberto Conconi[1,2], Niccolò Magnani[1], Stefano Zanchetta[1], and Michael Abratis[3]

[1]*Department of Earth and Environmental Sciences, University of Milano-Bicocca, Piazza della Scienza 4, Milano 20126, Italy*
[2]*Unité Matériaux et Transformations, Université de Lille, Citè Scientifique bâtiment C6, Villeneuve d'Ascq 59655, France*
[3]*Bruker Nano GmbH, Am Studio 2D, Berlin 12489, Germany*

***Corresponding author:** Giancarlo Capitani, E-mail: giancarlo.capitani@unimib.it

Abstract

The performance of an integrated parallel beam wavelength-dispersive/energy-dispersive microanalysis system mounted on a field emission scanning electron microscope has been compared with that of a conventional electron microprobe, using the same reference samples and as close as possible operational conditions. Tests on standards of known composition reveal internally consistent results for the former, and no obvious advantage of wavelength-dispersive over energy-dispersive spectroscopy has emerged for major elements without peak overlaps. Rather, because an energy-dispersive spectrometer can acquire all energies of the X-ray spectrum concurrently, conveying a lower electron dose per atom, it has the advantage of being faster and milder to minerals. In all cases, however, element migration may be significant, especially for monovalent, large ionic radius elements such as K and Na.

Key words: EDS, electron probe microanalysis, parallel beam WDS

Introduction

Electron probe microanalysis (EPMA) based on wavelength-dispersive spectroscopy (WDS) is one of the widely used analytical techniques employed in Earth Sciences to achieve quantitative chemical compositions at the microscale of major and minor elements. In a WDS system, a diffractor exploits Bragg's law to select desired X-ray wavelengths (λ) from the different elements in the sample. The photons so selected are then detected by a proportional counter. In a conventional WD spectrometer, the X-ray source on the sample, the diffractor and the detector are located on an imaginary Rowland circle, where the source-to-diffractor distance is a linear function of λ. The required Bragg condition for the desired λ is obtained by moving the diffractor along a linear track aligned with the X-ray source (Fig. 1). To cover all the possible wavelengths of the analyzed elements, several diffractors with different lattice spacings are commonly mounted in a spectrometer and several spectrometers (usually from three to five mounted around the electronic column) working in synchronous are usually employed to speed up the analysis.

In the late 1990s, compact WDS systems for integrated wave-dispersive/energy-dispersive (hereafter WEDS) analysis in a scanning electron microscope (SEM) became commercially available. The parallel beam design satisfies the typically lower beam currents and various chamber designs on various SEMs. Moreover, it is acknowledged that WDS performs better for light elements (i.e., lighter than Si) than EDS and also that it is accounted for higher sensitivity, ~0.03 Wt.% versus ~0.1 Wt.% under routine conditions (i.e., 15–20 keV, 5–20 nA, 1–3 μm spot size, 10–20 s counting time for peak; Reed, 2010). As a consequence, WEDS systems have been developed according to two opposite philosophies: (i) using parallel beam WDS to measure light elements and EDS to measure heavy elements and (ii) using Rowland circle WDS to measure trace elements and EDS for major elements (Fig. 2). Because of the different construction geometry (Fig. 3), the parallel beam WDS is more compact and in principle is more efficient because the collimator moves closer to the sample, but it can be limited in energy to less than 4 keV—as for the model used here (Bruker XSense)—whereas the Rowland circle WDS can span the energy range typically up to 10 keV, as for a dedicated EPMA. Currently, on the market, there are two other parallel beam WDS systems—i.e., Thermo Scientific MagnaRay and EDAX Lambda—which can span the entire energy range as for the Rowland circle WDS, at cost of spectral resolution (e.g., Seddio, 2019). These compact WEDS integrated systems are commercially very attractive because they may allow EPMA capabilities in an in-house SEM, for instance, with about one fifth of the budget required for a dedicated EPMA.

In this work, we compared the performance of a compact, integrated parallel beam WEDS microanalysis system with that of a pure EDS system, using conventional EPMA data as a reference. All analyses were performed on the same thin sections, positioning the electron beam as close as possible to reference points (i.e., where the EPMA analyses where done), but avoiding direct superposition on already excited sample volumes. Operational conditions were set to be similar in all the experimental routines. Moreover, any analytical difference introduced on the analysis by the different source used, i.e., field emission gun (FEG) source or a conventional thermionic (tungsten) source, is discussed.

Received: April 28, 2025. **Revised:** September 9, 2025

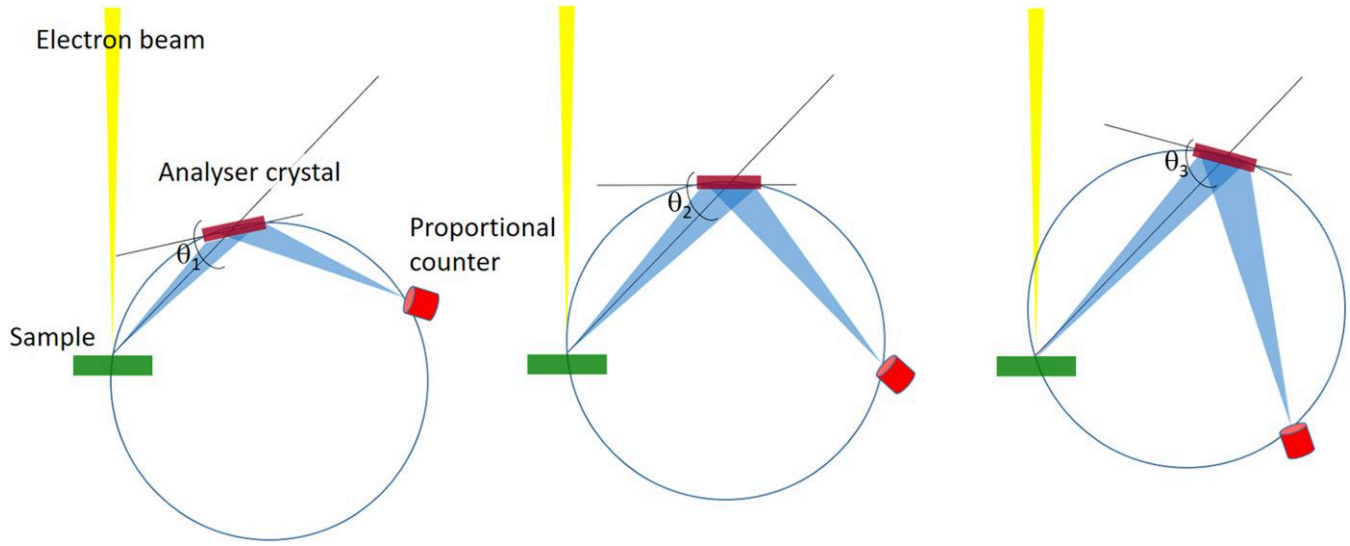

Fig. 1. Schematic Rowland circle geometry of a classical WDS for three different Bragg positions: the wavelength of the analyzed element increases from left to right.

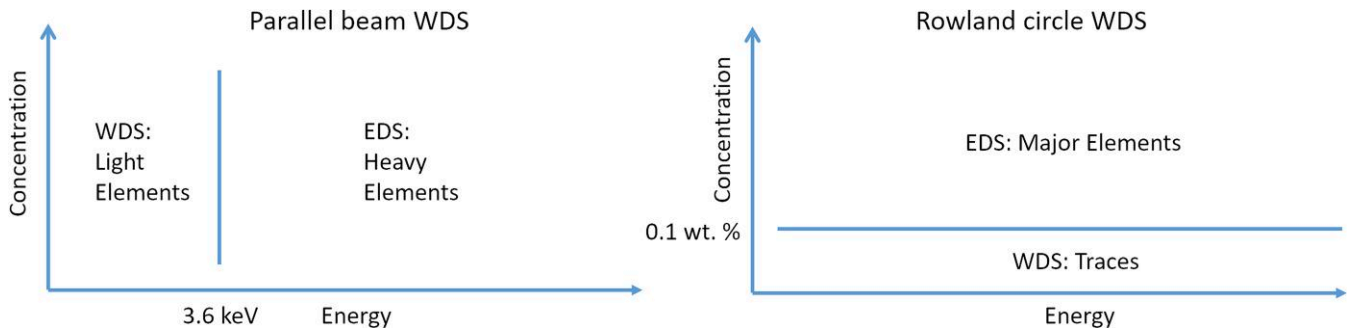

Fig. 2. Conceptual diagrams showing the different analytical approaches of integrated WEDS systems: parallel beam WDS (left) and Rowland circle WDS (right).

Instruments and Samples

EDS and WEDS analyses were conducted at the Platform of Microscopy of the University of Milano-Bicocca (PMiB) with a FEG-SEM Zeiss Gemini 500, equipped with a Bruker XFlash 6|30 EDS detector (nominal sensitive area 30 mm^2) and a Bruker XSense parallel beam QUANTAX WDS detector. The instrument was operated at 15 keV, with a beam current of 19 nA (measured by a Faraday cup), an analytical working distance of 8.18 mm, and a magnification of 2500X. Under these conditions, the beam size diameter, estimated experimentally (e.g., Larionov, 2014), was ~60 nm. For WDS analyses, the counting time was set to 60 s for peak and 30 s for background, which typically yielded 44,000–150,000 background-corrected counts for major elements (Si and Al), depending on element abundance in the different minerals. For Fe *Lα*, a counting time of 120 s for peak and 60 s for background was used, which typically yielded 500–4,600 background-corrected counts (Supplementary Table S1 in the Supplementary Material). The background was measured at positions suggested by the program, the same for standards and unknowns, on the left and right sides of the peak, after verified by a WDS scan that no other peak interfered with the measured positions. Then, a linear interpolation was used to remove background. For EDS, the counting time was 60 s and the background subtraction (determined automatically) was checked in the interactive dialog of the quantification software and adjusted if necessary. Data acquisition and processing were undertaken with the Bruker Esprit 2.5 software. In order to avoid saturation, the detector was kept in a retracted position during the analysis. The processing time was selected automatically by the program, which typically yielded a dead time between 15 and 33% and a counting rate typically of ~57–72 kcps.

Both EDS and WDS systems were calibrated simultaneously using natural mineral standards provided by Astimex Standards Ltd., whose quality has been proven by years of use in two different laboratories: albite (Na, Al, Si, Ca), almandine (Mg, Ca, Mn, Fe), biotite (Mg, Al, Si, K, Ca, Mn, Ti, Fe), chlorite (Ca, Cr), Cr-diopside (Cr, Fe), diopside (Mg, Ca, Ti, Mn), jadeite (Na, Al, Si), kaersutite (Na, Mg, Al, Si, Ca, Mn, Fe), pyrope (Al, Si, Ti, Cr), rhodonite (Mn), and sanidine (K); synthetic C_2O_3 (Cr) was also used. In WDS mode, the Fe *Lα*, Na *Kα*, Mg *Kα*, and Al *Kα* were measured with the TAP crystal (thallium acid phthalate, $d = 12.95$ Å); the K *Kα* and Si *Kα* were measured with the PET crystal (pentaerythritol, $d = 4.371$ Å). In EDS mode, *K*-lines were used for all elements. Oxygen was determined by stoichiometry. Additionally, to

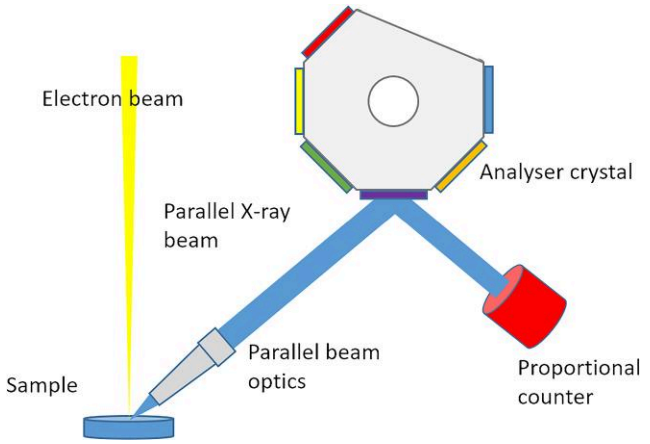

Fig. 3. Schematic representation of a parallel beam WDS mounting up to six crystals in a single spectrometer.

minimize sample damage and migration (e.g., Nielsen & Sigurdsson, 1981; Morgan & London, 1996; 2005; McCubbin et al., 2010) of monovalent cations such as Na and K, for albite, biotite, and chlorite, a calibration with a defocused beam (for both EDS and WDS) was performed, analyzing an area of $\sim 1\ \mu m^2$. Defocusing was achieved acquiring the analyses at the analytical working distance and scanning the beam over an area of $\sim 1.3\ \mu m \times 0.8\ \mu m$.

EPMA analyses were performed at the Department of Earth Science "Ardito Desio" of the University of Milan, using a JEOL JXA-8200 WDS EPMA, and processed with the JEOL software. These analyses were acquired with an accelerating voltage of 15 keV, a beam current of ~5 nA, a spot size of 5 μm for mica, and ~1 μm for all the other minerals. Acquisition time was 30 s for the peak and 10 s for each (left and right) background, which was removed by linear interpolation. The following standards were used: K-feldspar (K), albite (Na), olivine (Mg, Fe), grossular (Ca, Al, Si), rhodonite (Mn), amphibole (Ti), and chromite (Cr). These are "homemade" standards whose quality has never been questioned in decades of intensive use.

The composition of five different minerals was investigated: three nominally anhydrous phases (garnet, clinopyroxene, and plagioclase) and two hydrous phases (amphibole and white mica). Specifically, plagioclase was sourced from the Tanno pegmatite (Central Alps). The Tanno pegmatite belongs to the most differentiated class of pegmatites and to the LCT (lithium, cesium, tantalum) petrogenetic family (Arrigoni et al., 2020). The plagioclase in these pegmatites occurs as large crystals, reaching centimetric scales, and exhibits a nearly pure albitic composition.

The analyzed amphibole, garnet, clinopyroxene, and white mica come from eclogites of the Adula nappe in the San Bernardino Pass area (South Switzerland, Central Alps). The eclogites occur as meter- to decameter-sized boudins enclosed in paragneiss at the top of the Adula nappe, close to the contact with the Misox Zone (Pleuger et al., 2003). The eclogites primarily consist of garnet, Na-clinopyroxene, phengitic white mica, and quartz in varying proportions (Pleuger et al., 2003). Na-Ca amphibole grows syn- to post-kinematically with respect to the eclogite foliation. Rutile, zoisite, plagioclase, chlorite, apatite, and zircon occur in accessory quantities. Eclogites have a mylonitic texture marked by the shape preferred orientation of omphacitic clinopyroxene and phengitic white mica. A well-developed compositional layering marked by alternating clinopyroxene-rich and garnet-rich levels occurs in some boudins. Garnets are predominantly a solid solution of almandine, grossular, and pyrope, with a prevalent almandine composition. Occasionally, weak zoning is observed, with the core enriched in grossular and the rim showing an enrichment in pyrope. Amphiboles belong to the Na-Ca group, while white mica is primarily phengitic (Pleuger et al., 2003).

The EPMA and WEDS analyses were performed on 30 μm thick polished thin sections, following detailed petrographic characterization under the optical microscope. Before analysis, they were coated with a 20 nm C-film to prevent electrostatic charging under the electron beam.

Results and Discussion

Parallel Beam WEDS Standardization

To verify the reproducibility and accuracy of the standardization, from five to ten spot analyses were carried out on the same standard minerals used for calibration. The results were then quantified using the $\phi(\rho z)$ correction method based on the XPP algorithm (Pouchou & Pichoir, 1991; Newbury & Ritchie, 2015; 2019). Table 1 reports the compositions of three standard samples: pyrope, albite and biotite, along with the results of the quantification with WEDS and EDS of the same spot analyses. The results demonstrate the accuracy and the reproducibility of both methods, as the measured values closely align with the standard compositions. Figure 4 represents the reproducibility of the measurements by plotting the calculated standard deviations for each analyzed oxide. It can be seen that in the case of pyrope, EDS results yield standard deviations slightly lower than for WEDS for almost all analyzed oxides, whereas for all the other mineral standards, the results are similar, except for some pathological cases such as K_2O and FeO in biotite, for the reasons explained below. Figure 5 represents the accuracy of the measurements by showing the deviation (%) of the measured oxides after standardization from the nominal standard compositions. As can be seen, major deviations concern only minor elements, with the exception, again, of K_2O and FeO in biotite and Na measured by EDS in albite.

In albite, K is underestimated by WEDS, whereas in biotite it is overestimated, with a standard deviation of 1.4 (12%, see Table 1). A possible explanation for these anomalies is the migration of K during the extended time required for the WDS analysis. In WEDS mode, EDS spectra are collected in 60 s, whereas in WDS, each element is measured sequentially and a single analysis in albite and biotite can last up to 6 and 8 min, respectively. Thus, given the high current used (19 nA), K migration becomes likely, leading to inaccurate quantification. This issue is minimized in EDS mode due to its shorter analysis time (60 s). To address this problem, a second calibration and analysis in defocused mode (over an area of $\sim 1\ \mu m^2$) was performed on biotite to reduce K migration. In this case, the results show a better match between the nominal standard composition and both WEDS and EDS results, suggesting that the migration of K was caused by the prolonged acquisition time and high current employed by the WDS system in spot mode.

To further constrain this issue, we performed additional tests: (i) we repeated the analyses (and standardization) carefully placing K at the beginning of the measuring sequence and (ii) we performed time dependent intensity (TDI)

Table 1. Comparison Between the Nominal Compositions and the Analytical Results Obtained With Both WEDS and EDS Systems.

	Pyrope	WEDS(10)	SD	EDS(10)	SD	Albite	WEDS(5)	SD	EDS(5)	SD
Na_2O	-	-	-	-	-	11.59	11.46*	0.40	10.72	0.53
MgO	19.33	19.33*	0.14	19.15	0.06	-	-	-	-	-
Al_2O_3	21.32	21.13*	0.24	21.15	0.05	19.54	19.74*	0.14	19.72	0.13
SiO_2	41.45	41.53*	0.26	41.53	0.10	68.52	68.02*	0.28	68.89	0.28
K_2O	-	-	-	-	-	0.22	0.16*	0.05	0.23	0.03
CaO	4.65	4.77	0.04	4.79	0.03	0.13	0.09	0.07	0.09	0.07
TiO_2	1.16	1.20	0.03	1.21	0.03	-	-	-	-	-
Cr_2O_3	0.58	0.54	0.02	0.54	0.02	-	-	-	-	-
MnO	0.27	0.34	0.03	0.34	0.03	-	-	-	-	-
FeO	11.15	10.80*	0.28	11.24	0.04	-	-	-	-	-
Σ	99.9	99.64	0.30	99.95	0.19	100.00	99.47	0.24	99.67	0.23
	Biotite	WEDS(10)	SD	EDS(10)	SD	Biotite[d]	WEDS(6)	SD	EDS(6)	SD
MgO	19.52	18.98*	0.22	18.98	0.24	19.52	19.59*	0.40	19.03	0.28
Al_2O_3	15.13	14.79*	0.42	14.99	0.28	15.13	15.00*	0.18	14.85	0.26
SiO_2	38.72	38.02*	0.69	38.11	0.50	38.72	38.47*	0.28	38.13	0.48
K_2O	9.91	11.96*	1.44	10.67	0.67	9.91	9.30*	0.75	9.88	0.04
CaO	0.10	b.d.l.	-	b.d.l.	-	0.10	b.d.l.	-	b.d.l.	-
TiO_2	1.77	1.64	0.17	1.62	0.17	1.77	2.11	0.31	2.11	0.31
MnO	0.04	0.02	0.00	0.02	0.00	0.04	0.04	0.00	0.04	0.00
FeO	10.72	10.28*	0.35	10.53	0.16	10.72	10.97*	0.51	10.78	0.07
Σ	95.91	95.69	0.69	94.92	0.80	95.91	95.48	0.85	94.82	0.66

Pyrope, albite, and biotite were used as standards (number of averaged analyses in brackets; SD, standard deviation). Biotite analyses were carried out both in spot and defocused beam (biotite[d]) mode, in order to evaluate the behavior of element diffusion. In WEDS mode, Na *Kα*, Mg *Kα*, Al *Kα*, Si *Kα*, K *Kα*, and Fe *Lα* were measured with WDS (*); all the other elements with EDS; b.d.l., below detection limit.

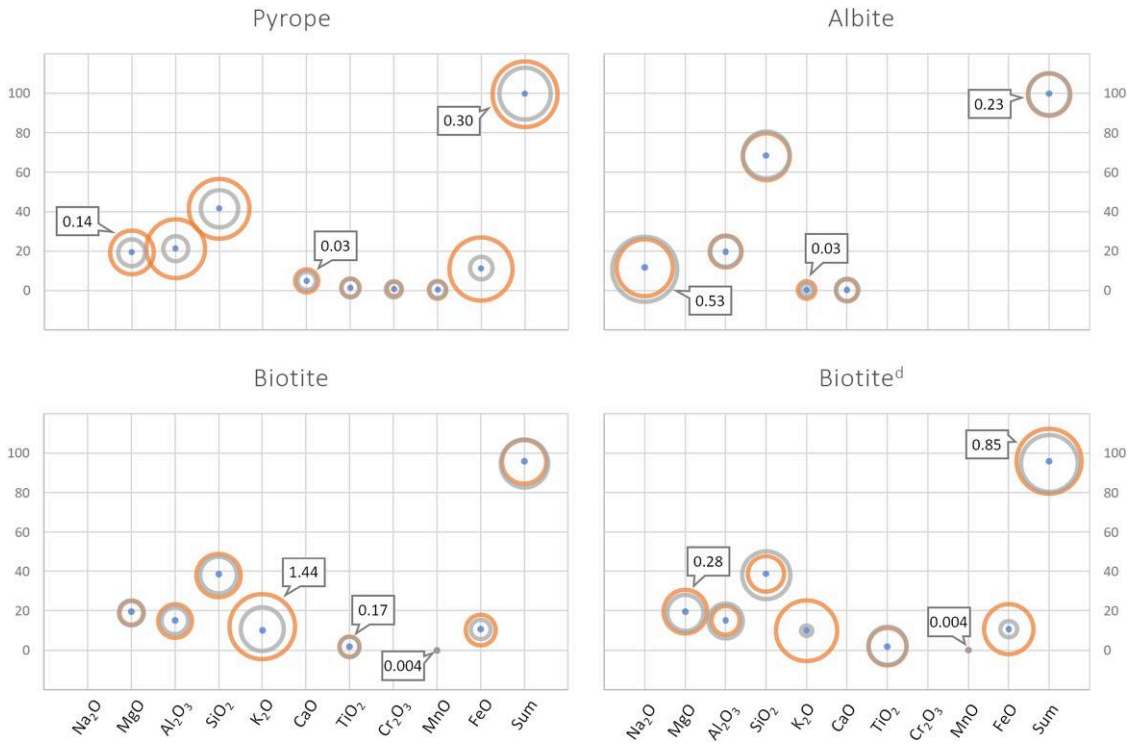

Fig. 4. Synoptic representation of the reproducibility of the measurements plotting the standard deviations reported in Table 1 for WEDS (orange) and EDS (gray): pyrope (upper left), albite (upper right), biotite (lower left), and biotite analyzed with defocused beam (lower right). Bubbles are centered on the average value of the relative oxide and their area is proportional to the standard deviation (some values labeled as size guide). The point at the center of the bubbles represents the nominal composition of the standard.

measurements (Nielsen & Sigurdsson, 1981; McCubbin et al., 2010; Donovan et al., 2021). Putting K at the beginning of the analysis sequence did not significantly improve the results. A possible explanation is suggested by the TDI tests themselves, which revealed that migration is more severe than expected, and affects as well K as Na (Supplementary Figs. S1 and S2 and Tables S2 and S3 in the Supplementary Material). Basically, K migration occurs in the first seconds of the

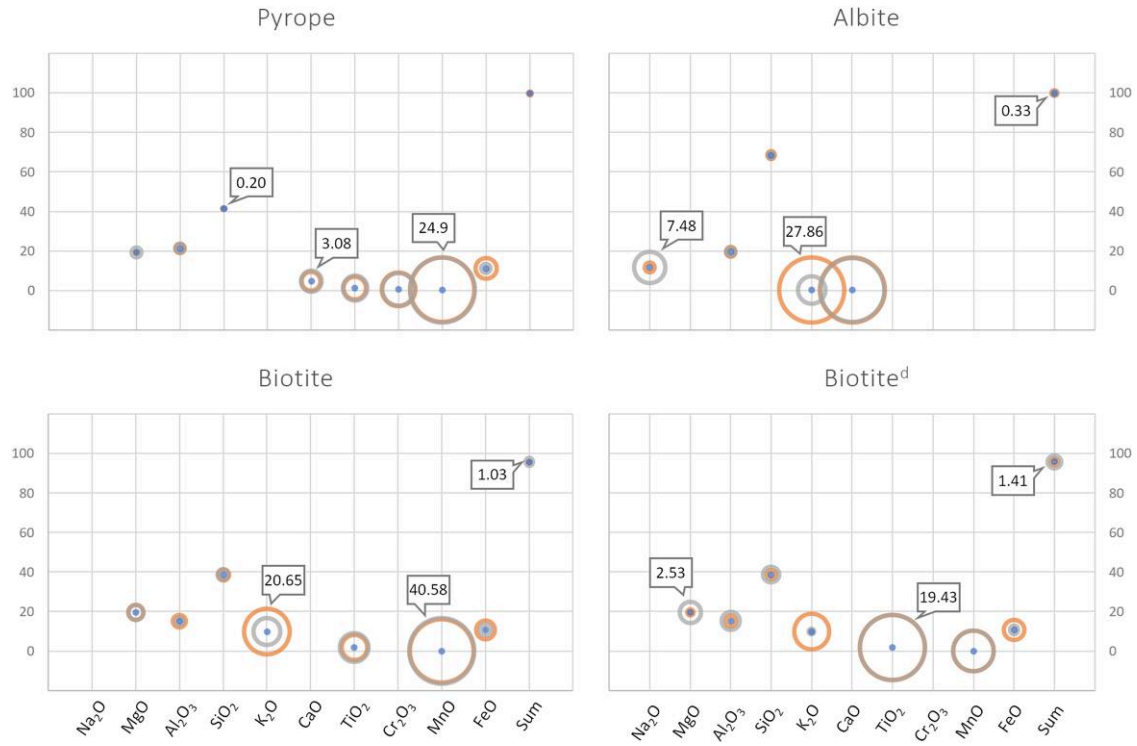

Fig. 5. Synoptic representation of the accuracy of the measurements plotting the deviation (%) of the WEDS (orange) and EDS (gray) results from the nominal composition of standards: pyrope (upper left), albite (upper right), biotite (lower left), and biotite analyzed with defocused beam (lower right). Bubbles are centered on the average value of the relative oxide and their area is proportional to the deviation from the standard composition (some values labeled as size guide). The deviation (%) is defined as | (standard value - WEDS value (or EDS value)) |/standard value*100. The point at the center of the bubbles represents the nominal composition of the standard.

analysis; therefore, 60 s is already a too long time to avoid migration. However, repeated measurements (and standardization) with a more defused beam, selected following the indications of TDI tests, did not improve significantly the results either. A possible lesson we can draw from these observations is that if standardization and measurements are done in the same manner (same beam energy, current, size, acquisition time, etc.) and standards and unknowns have similar composition (and structure?), migration effects, at least in part, cancel out. On the other hand, augmenting the defocus will decrease the spatial resolution, making the application of WDS of less wide interest.

The poorer reproducibility of Fe by WEDS is likely due to anomalous absorption of the Fe *Lα* line (e.g., Gopon, 2016; Buse & Kearns, 2018; Moy et al., 2019; 2022). Briefly, the mass absorption coefficient of the Fe *Lα* line changes with material making matrix correction inaccurate, resulting in a higher standard deviation than for EDS, where the Fe *Kα* is used, which is not affected by this problem.

Application to Some Reference Samples

In order to compare EDS and parallel beam WEDS systems with each other and with the EPMA system, analyses were performed on samples previously analyzed using the latter. The analyzed minerals were garnet, pyroxene, amphibole, albite, and white mica. Additionally, different quantification procedures were compared in the EDS and WEDS systems:

- Procedure (I): Quantification using the same (or very similar) standards employed in EPMA analysis. The following standards were used: pyrope (Al, Si), synthetic Cr_2O_3 (Cr), almandine (Ca, Mg, Fe), sanidine (K), albite (Na), kaersutite (Ti), and rhodonite (Mn).
- Procedure (II): Quantification using, whenever possible, standards similar to the analyzed minerals. For instance, pyroxene standards were used for pyroxene analyses, feldspar standards were used for albite analyses, etc. Details for each mineral are provided in the following sections.
- Procedure (III): Quantification for minerals containing monovalent cations, using a defocused beam for calibration and analysis. See the white mica section for further details.

Garnet

Table 2 reports garnet analyses obtained by EPMA, WEDS, and EDS. WEDS and EDS results are reported for two different quantification procedures, (I) and (II). For procedure (II), garnet standards were employed: pyrope (Al, Si, Ti, Cr) and almandine (Mg, Ca, Mn, Fe).

From a taxonomic point of view, the garnet is almandine with grossular and pyrope components and very minor spessartite (Fig. 6). All analyses show a good agreement with the ideal garnet composition ($A_3B_2Si_3O_{12}$), with only minimum variations, always within 1.6%.

As expected, the two different quantification procedures did not yield significantly different results, since the most concentrated elements are quantified using the same standards (pyrope and almandine) in both procedures (I) and (II). However, WEDS analyses more closely match the EPMA analyses compared to

Table 2. Comparison Among the EPMA (Single Spot; Er% = 1σ Relative Error), WEDS, and EDS Analyses of Garnet.

	EPMA	Er%	WEDS(I)	SD	EDS(I)	SD	WEDS(II)	SD	EDS(II)	SD
MgO	4.68	1.63	4.77*	0.38	5.98	0.33	4.77*	0.38	5.98	0.33
Al_2O_3	22.03	0.60	21.52*	0.10	21.58	0.05	21.52*	0.10	21.58	0.05
SiO_2	39.30	0.45	39.04*	0.21	38.52	0.04	39.04*	0.21	38.52	0.04
CaO	7.43	0.72	7.57	0.37	7.59	0.37	7.57	0.37	7.59	0.37
TiO_2	0.04	87.4	0.10	0.08	0.10	0.09	0.11	0.09	0.11	0.09
MnO	0.38	9.71	0.42	0.13	0.44	0.05	0.42	0.13	0.44	0.05
FeO	28.96	0.70	27.52*	0.48	25.98	0.65	27.52*	0.48	25.98	0.65
$\sum$	102.82		100.94	0.19	100.20	0.13	100.95	0.20	100.20	0.13
Mg	0.533		0.551		0.692		0.551		0.692	
Al	1.983		1.965		1.975		1.964		1.975	
Si	3.002		3.024		2.990		3.024		2.990	
Ca	0.608		0.628		0.631		0.628		0.631	
Ti	0.002		0.006		0.006		0.007		0.007	
Mn	0.025		0.027		0.029		0.027		0.029	
Fe	1.850		1.783		1.687		1.783		1.687	
$\sum_A$	3.016		2.990		3.038		2.990		3.039	
$\sum_B$	1.986		1.971		1.981		1.971		1.982	
$\sum_{All}$	8.004		7.985		8.009		7.985		8.010	

In WEDS mode, Mg *Kα*, Al *Kα*, Si *Kα*, and Fe *La* were measured with WDS (*); all the other elements with EDS. (I) and (II) represent the two different quantification procedures used. Reported compositions are the average of three spot analyses (SD, standard deviation). Upper columns: oxide Wt.%; lower columns: atoms per formula unit (a.p.f.u.) calculated on a base of 12 oxygens. $\sum_A$ = Mg + Ca + Mn + Fe; $\sum_B$ = Al + Ti; $\sum_{All}$ = sum of all cations.

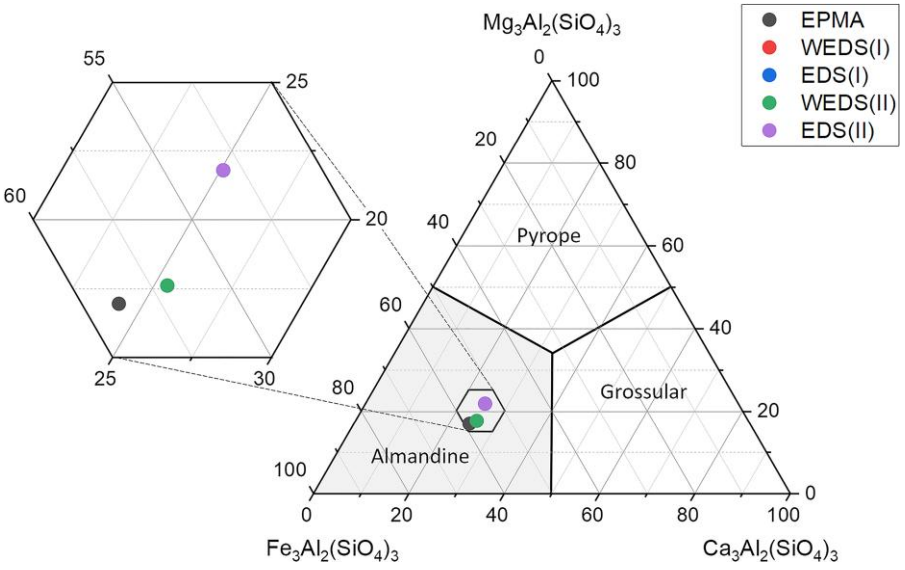

Fig. 6. Compositional ternary plot of the analyzed garnet (after Grew et al., 2013). WEDS(I) and WDS(II) are practically superposed, as well as EDS(I) and EDS(II).

the EDS results. Indeed, the amount of Fe is slightly underestimated with EDS. As regards the total oxides, the ideal closure of garnet (100%) is more closely approached by EDS (100.20) and WEDS (100.94) than by EPMA (102.82). All methods provide reliable results in terms of stoichiometry. Finally, the quite high standard deviations for Ca, Mg, and Fe affecting the WEDS and EDS analyses may be attributed to the fine scale zoning affecting garnet, even if we tried to minimize the problem by setting the analyzed spots within the core of the crystal.

Clinopyroxene

Table 3 reports clinopyroxene analyses obtained using EPMA, WEDS, and EDS. WEDS and EDS results are reported for two different quantification procedures, (I) and (II). For procedure (II), clinopyroxene standards were employed: jadeite (Na, Al, Si), diopside (Mg, Ca, Ti, Mn), and Cr-diopside (Cr, Fe).

Pyroxenes show extensive solid solutions caused by various ionic substitutions. According to the classification by Morimoto (1988), the general pyroxene formula is $M2M1T_2O_6$, where M2 and M1 represent cations in distorted and regular octahedral coordination, respectively, and T represents tetrahedrally coordinated cations. The analyzed clinopyroxene is a Ca-Na pyroxene with omphacitic composition (Fig. 7). In comparison to EPMA analysis, the EDS(I) and WEDS(I) analyses show an overestimation of Na and an underestimation of Al, which globally result in an excess of M2 cations and total cations. This moves the overall compositions, once estimated the Fe^{3+} content through Droop (1987), toward the aegirine-augite field, almost swapping the proper classification. EDS(II) and WEDS(II) analyses compare better with the EPMA analysis, apart from a minor underestimation of Fe with WEDS(II) and overestimation of

Table 3. Comparison Among the EPMA (Single Spot; Er% = 1σ Relative Error), WEDS, and EDS in Clinopyroxene Analysis.

	EPMA	Er%	WEDS(I)	SD	EDS(I)	SD	WEDS(II)	SD	EDS(II)	SD
Na_2O	7.74	1.53	10.84*	0.09	9.34	0.09	7.85*	0.07	7.33	0.07
MgO	7.16	1.23	5.86*	0.06	7.29	0.03	6.77*	0.07	6.64	0.02
Al_2O_3	12.20	0.79	10.90*	0.06	11.77	0.10	13.15*	0.07	13.86	0.12
SiO_2	56.94	0.36	55.38*	0.16	54.56	0.04	56.74*	0.16	54.44	0.04
CaO	11.48	0.57	11.04	0.07	11.33	0.06	10.65	0.06	10.90	0.06
TiO_2	0.10	31.3	0.12	0.02	0.12	0.02	0.63	0.09	0.65	0.09
Cr_2O_3	0.04	96.4	0.01	0.01	0.01	0.01	0.01	0.01	0.01	0.01
MnO	0.11	23.4	0.01	0.01	0.01	0.01	0.03	0.02	0.03	0.02
FeO	5.84	1.63	5.99*	0.33	5.19	0.05	4.60*	0.26	5.22	0.05
$\sum$	101.62		100.14	0.26	99.62	0.10	100.42	0.17	99.07	0.13
Na	0.526		0.758		0.653		0.535		0.509	
Mg	0.374		0.315		0.391		0.355		0.354	
^{T}Al	0.003		0.002		0.034		0.005		0.049	
^{M}Al	0.501		0.461		0.466		0.539		0.536	
Si	1.997		1.998		1.966		1.995		1.951	
Ca	0.431		0.427		0.437		0.401		0.418	
Ti	0.003		0.003		0.003		0.017		0.017	
Cr	0.001		0.000		0.000		0.000		0.000	
Mn	0.003		0.000		0.000		0.001		0.001	
Fe	0.171		0.181		0.156		0.135		0.156	
$\sum_{M2}$	0.961		1.186		1.091		0.938		0.929	
$\sum_{M1}$	1.050		0.961		1.017		1.046		1.065	
$\sum_{T}$	2.000		2.000		2.000		2.000		2.000	
$\sum_{All}$	4.011		4.146		4.107		3.984		3.994	

In WEDS mode, Na *Kα*, Mg *Kα*, Al *Kα*, Si *Kα*, and Fe *Lα* were measured with WDS (*); all the other elements with EDS. (I) and (II) represent the two different quantification procedures used. Reported compositions are the average of three spot analyses (SD, standard deviation). Upper columns: oxide Wt.%; lower columns: atoms per formula unit (a.p.f.u.) calculated on a base of six oxygens. $\sum_T$ = Si + ^{T}Al; $\sum_{M1}$ = ^{M}Al + Mg + Ti + Cr + Fe; $\sum_{M2}$ = K + Na + Ca + Mn; $\sum_{All}$ = sum of all cations.

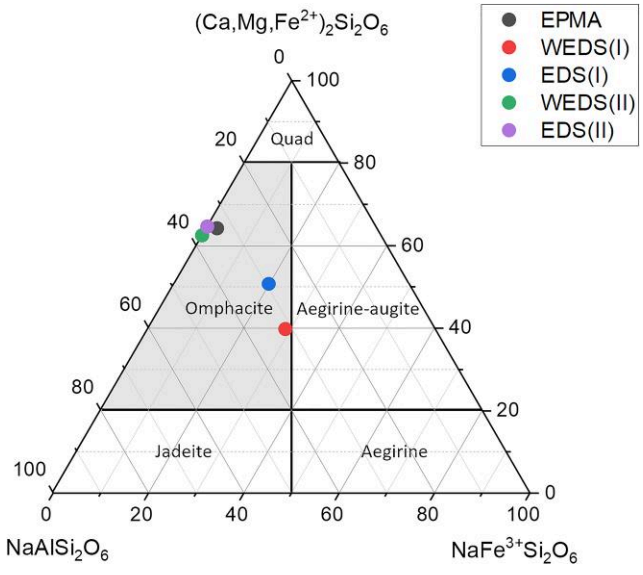

Fig. 7. Compositional ternary plot of the analyzed clinopyroxene. Quad represents Ca-Mg-Fe clinopyroxenes (after Morimoto, 1988). The Fe^{3+} content was estimated according to Droop (1987).

Al with EDS(II). Overall, with the procedure (II), the derived crystal chemistry compares well with ideal pyroxene composition, assuming that part of the Fe, attributed to the M1 sites, could occupy in part the M2 site. As assumed above, the underestimation of Fe in WEDS mode may be due to anomalous absorption of the Fe *Lα* line (e.g., Gopon, 2016; Buse & Kearns, 2018; Moy et al., 2019; 2022).

The discrepancy affecting the Na quantification between the two procedures is likely due to the standards used. Indeed, in procedure (I), albite was used as standard for Na, as was also the case for the EPMA analysis. In procedure (II), jadeite was employed. The difference in Na values between the two procedures may be attributed to the different tendency of Na to migrate in albite and jadeite. Consequently, a higher migration of Na during standardization in albite, compared to jadeite, could result in an overestimation of Na during quantification. This problem did not occur with EPMA, because of the lower current (5 nA) used and the larger probe size (~1 μm), as compared to WEDS analysis (19 nA and 60 nm, respectively). Indeed, although the interaction volume calculated with CASINO (Drouin et al., 2007) for EPMA and WEDS is comparable (Supplementary Fig. S4 in the Supplementary Material), the electron density at the sample surface is about 260 times higher for the latter! Morgan and London (2005) measured that significant Na loss occurred in alkali aluminosilicate glasses using current densities of ~0.1–0.2 nA/μm^2. Even though here we are dealing with crystalline materials, where cations are expectably more tightly bonded to the structure than in glass, the electron density involved is two orders of magnitude higher; therefore, alkali migration is very likely. Our TDI tests actually confirm that alkali migration is a severe problem even in crystalline materials (Supplementary Figs. S1 and S2 and Tables S2 and S3 in the Supplementary Material).

Amphibole

Table 4 reports amphibole analyses obtained by EPMA, WEDS, and EDS. For quantification following procedure (II), amphibole standards were used whenever possible. Thus, the following standards were employed: kaersutite (Na, Mg, Ti, Al, Si, K, Ca, Mn, Fe) and pyrope (Cr).

Amphiboles typically exhibit complex chemical formulas and variable compositions, often forming intricate solid

Table 4. Comparison Among the EPMA (Single Spot; Er% = 1σ Relative Error), WEDS, and EDS Systems in Amphibole Analysis.

	EPMA	Er%	WEDS(I)	SD	EDS(I)	SD	WEDS(II)	SD	EDS(II)	SD
Na_2O	5.28	1.93	7.24*	0.09	5.77	0.23	4.83*	0.06	4.19	0.17
MgO	11.42	0.97	10.01*	0.10	12.29	0.10	11.17*	0.11	11.25	0.09
Al_2O_3	14.74	0.74	13.90*	0.17	14.39	0.07	13.571*	0.17	13.79	0.06
SiO_2	48.24	0.40	49.34*	0.17	48.08	0.08	49.39*	0.17	48.65	0.08
K_2O	0.38	4.05	0.46	0.00	0.46	0.00	0.34	0.00	0.34	0.00
CaO	6.51	0.77	6.34	0.06	6.34	0.06	6.30	0.06	6.29	0.06
TiO_2	0.42	9.39	0.43	0.01	0.43	0.01	0.43	0.01	0.43	0.01
MnO	0.03	88.0	0.03	0.01	0.03	0.01	0.04	0.02	0.04	0.02
FeO	11.39	1.14	11.02*	0.15	10.60	0.02	10.40*	0.10	11.39	0.02
$\sum$	98.41		98.77	0.39	98.39	0.34	96.46	0.38	96.37	0.27
^{A}Na	0.569		0.748		0.683		0.367		0.329	
^{B}Na	0.883		1.243		0.905		0.975		0.841	
Mg	2.415		2.116		2.599		2.387		2.416	
^{T}Al	1.156		1.002		1.180		0.920		0.992	
^{C}Al	1.309		1.322		1.226		1.373		1.349	
Si	6.844		6.998		6.820		7.080		7.008	
K	0.069		0.083		0.083		0.062		0.062	
^{B}Ca	0.990		0.757		0.964		0.967		0.970	
^{C}Ca	0.000		0.206		0.000		0.000		0.000	
Ti	0.045		0.046		0.046		0.046		0.047	
Mn	0.004		0.003		0.003		0.005		0.005	
^{B}Fe	0.123		0.000		0.129		0.053		0.184	
^{C}Fe	1.228		1.308		1.129		1.194		1.188	
$\sum_A$	0.638		0.831		0.767		0.429		0.391	
$\sum_B$	2.000		2.000		2.000		2.000		2.000	
$\sum_C$	5.000		5.000		5.000		5.000		5.000	
$\sum_T$	8.000		8.000		8.000		8.000		8.000	
$\sum_{All}$	15.638		15.831		15.767		15.429		15.391	

In WEDS mode, Na *Kα*, Mg *Kα*, Al *Kα*, Si *Kα*, and Fe *Lα* were measured with WDS (*); all the other elements with EDS. (I) and (II) represent the two different quantification procedures used. Reported compositions are the average of three spot analyses (SD, standard deviation). Upper columns: oxide Wt.%; lower columns: atoms per formula unit (a.p.f.u.) calculated on a base of 23 oxygens.
$\sum_A = {}^{A}Na + K$; $\sum_B = {}^{B}Na + Ca + Mn + {}^{B}Fe$; $\sum_C = {}^{C}Al + Mg + Ti + {}^{C}Fe$; $\sum_T = Si + {}^{T}Al$; $\sum_{All}$ = sum of all cations.

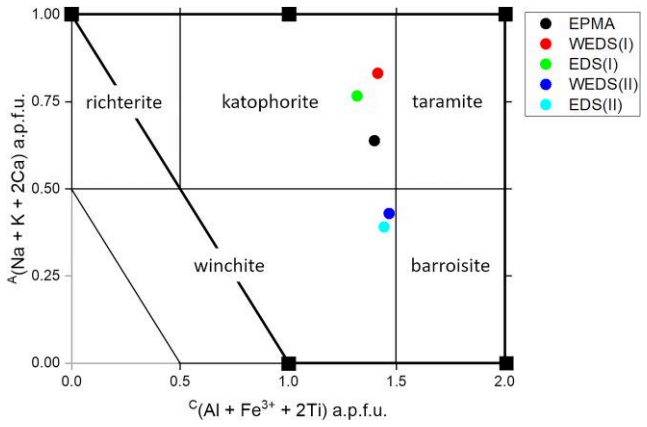

Fig. 8. Plot of the analyzed amphibole on the compositional diagram for Na-Ca-amphiboles (after Hawthorne et al., 2012). The heavy black lines represent a two-dimensional section of amphibole composition space at $^{B}Ca/^{B}(Ca + Na) = 0.5$ that contains the Na-Ca end-member compositions. The thin black lines show the possible range of amphibole compositions at $^{B}Ca/^{B}(Ca + Na) = 0.5$ and the solid lines to the left of the diagonal heavy black line show the possible range of amphibole compositions at $^{B}Ca/^{B}(Ca + Na) = 0.75$, the boundary between the Na-Ca-amphiboles and the Ca-amphiboles.

solutions. Consequently, assessing the quality of the analyses is not straightforward. The general amphibole formula is $A_{0\text{-}1}B_2C_5T_8O_{22}(OH,F)_2$, where A, B, and C represent the octahedral sites (A), (M4), and (M1, M2, and M3), respectively, and T represents the tetrahedral site. Generally, A = Na, K, Ca, Pb, Li; B = Na, Ca, Mg, Fe^{2+}, Mn, Li; C = Mg, Fe^{2+}, Fe^{3+}, Al, Mn, Li, Cr, Ti, Zn; and T = Si, Al and Ti (Leake et al., 1997; Hawthorne et al., 2012).

The analyzed amphiboles belong to the Na-Ca group, but its precise classification depends on the accuracy of the analytical results, provided that Fe^{3+} could not be estimated. EPMA and procedure (I) analyses fall within the katophorite field, ideally $Na(NaCa)(Mg_4Al)(Si_7Al)O_{22}(OH)_2$, which has 16 cations in the chemical formula; procedure (II) analyses fall within the winchite field $[\square(NaCa)(Mg_4Al)Si_8O_{22}(OH)_2]$, which has ideally 15 cations because the A site is vacant (Fig. 8). All analyses (i.e., EPMA, WEDS, and EDS) yield cation sums between ~15.39 and ~15.83; therefore, the A site is only partially occupied by K and Na.

In comparison to EPMA, Na is overestimated with procedure (I) and underestimated with procedure (II). Considering the oxide totals, those determined by procedure (II) with both EDS and WEDS are lower than expected and partially attributable to the underestimation of Na and secondarily of Al. Moreover, WEDS and EDS yield slightly higher SiO_2 values and, in general, slightly higher SiO_2/Al_2O_3 ratios with both procedures. For the rest, WEDS(II) and EDS(II) are more similar to each other than WEDS(I) and EDS(I) and more similar to EPMA. The most striking results here is that, although a reasonable crystal chemical formula can be obtained with any procedure, significant differences arise as a function of the standards selected.

Albite

Table 5 reports albite analyses obtained by EPMA, WEDS, and EDS. For quantification following procedure (II), feldspar standards were used whenever possible. Thus, the following

Table 5. Comparison Among the EPMA (Single Spot; Er% = 1σ Relative Error), WEDS, and EDS Systems in Plagioclase Analysis.

	EPMA	Er%	WEDS(I)	SD	EDS(I)	SD	WDES(II)	SD	EDS(II)	SD
Na_2O	11.07	1.39	10.93*	0.17	7.96	0.16	11.88*	0.18	8.45	0.18
Al_2O_3	18.27	0.64	19.98*	0.06	20.68	0.12	20.15*	0.03	20.58	0.04
SiO_2	68.15	0.34	67.18*	0.03	69.20	0.38	65.75*	0.14	69.29	0.19
K_2O	0.19	6.22	0.17	0.01	0.18	0.01	0.16	0.01	0.16	0.01
CaO	1.12	2.01	1.07	0.02	1.10	0.03	1.18	0.03	1.15	0.02
FeO	0.06	46.6	0.00	0.00	0.01	0.00	0.00	0.00	0.00	0.00
Σ	98.86		99.33	0.24	99.14	0.45	99.11	0.07	99.63	0.19
Na	0.950		0.930		0.671		1.024		0.710	
Al	0.953		1.038		1.060		1.055		1.052	
Si	3.017		2.961		3.009		2.922		3.004	
K	0.011		0.009		0.010		0.009		0.009	
Ca	0.053		0.051		0.051		0.056		0.053	
Fe	0.002		0.000		0.000		0.000		0.000	
Σ_T	3.970		3.999		4.069		3.978		4.056	
Σ_M	1.017		0.990		0.733		1.089		0.773	
Σ_{All}	4.987		4.989		4.802		5.066		4.829	

In WEDS mode, Na *Kα*, Al *Kα*, and Si *Kα* were measured with WDS (*); all the other elements with EDS. (I) and (II) represent the two different quantification procedures used. Compositions are the average of three spot analyses (SD, standard deviation). Upper columns: oxide Wt.%; lower columns: atoms per formula unit (a.p.f.u.) calculated on a base of eight oxygens. $\sum_T$ = Si + Al; $\sum_M$ = Na + K + Ca + Fe ; $\sum_{All}$ = sum of all cations.

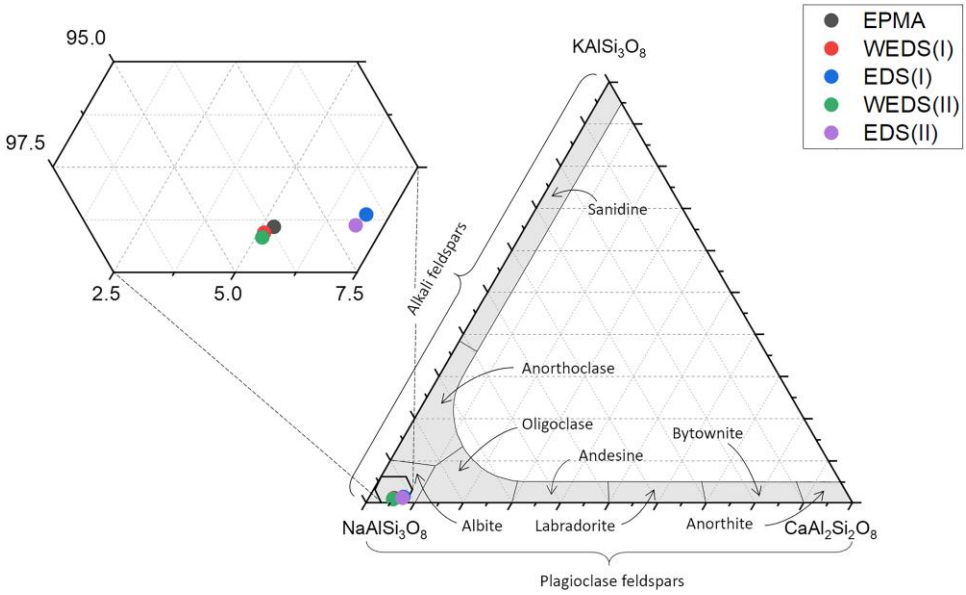

Fig. 9. Compositional ternary plot of the analyzed albite (after Smith, 1974).

standards were employed: albite (Na, Al, Si, Ca), almandine (Fe), and sanidine (K).

Feldspars have a general formula of MT_4O_8, where T represents Al^{3+} and Si^{4+} and M represents alkali and alkaline-earth atoms, such as Na^+, K^+, and Ca^{2+}. An extensive solid solution exists between Na and K (alkali feldspars) and between Na and Ca (plagioclases), whereas a limited solid solution exists between Ca and K (Fig. 9). If Ca^{2+} enters the structure substituting for Na (or K), an Al^{3+} substituting for Si^{4+} in T-sites is required to maintain charge balance, resulting in a coupled substitution $Ca^{2+} + Al^{3+} \leftrightarrow Na^+ + Si^{4+}$ (Deer et al., 2013). The EPMA analysis shows up to 0.053 a.p.f.u. of Ca that would require a corresponding excess of Al, which instead is underestimated (0.953 a.p.f.u.). In contrast, WEDS and EDS analyses show a very good correlation between Ca and Al. As far as Na is concerned, it appears well determined in EPMA and WEDS(I) analyses, but it is largely underestimated by EDS analysis, regardless of the quantification procedure used. This discrepancy, encountered also during the test on the albite standard (Table 1), can probably be explained with the high count rate, and consequent high dead time, of the EDS system. Actually, as clearly manifest in EDS spectra acquired in nominally Na-free minerals (biotite, Supplementary Fig. S3 in the Supplementary Material), a small peak at 1.050 keV and another small peak at 2.264 keV are visible, which can be interpreted, respectively, as the O *kα* + O *kα* and O *kα* + Si *kα* sum peaks, O and Si being the most intense peaks of the spectrum. Therefore, the underestimation of the Na peak may derive from an overcompensation of the 1.050 keV sum peak.

White Mica

Table 6 reports white mica analyses obtained by EPMA, WEDS, and EDS. For quantification following procedure

Table 6. Comparison Among the EPMA (Single Spot; Er% = 1σ Relative Error), WEDS, and EDS Analyses in White Micas.

	EPMA	Er%	WEDS(I)	SD	EDS(I)	SD	WEDS(II)	SD	EDS(II)	SD	WEDS(III)	SD	EDS(III)	SD
Na_2O	1.84	3.20	1.44*	0.03	1.26	0.04	1.44*	0.03	1.22	0.04	1.01*	0.04	3.49	0.09
MgO	2.12	2.25	2.04*	0.10	2.86	0.11	2.46*	0.11	2.98	0.11	2.34*	0.03	2.64	0.07
Al_2O_3	31.42	0.47	32.05*	0.11	32.37	0.14	32.23*	0.26	32.42	0.15	32.07*	0.57	30.59	0.23
SiO_2	49.29	0.39	52.64*	0.44	52.41	0.32	51.48*	0.09	51.44	0.31	54.02*	0.34	49.43	0.20
K_2O	8.65	0.69	3.56*	0.12	4.41	0.22	3.76*	0.14	5.00	0.25	2.88*	0.36	6.85	0.10
CaO	0.02	66.1	0.02	0.01	0.02	0.01	0.04	0.02	0.04	0.02	0.07	0.02	0.07	0.04
TiO_2	0.55	7.34	0.66	0.07	0.70	0.07	0.76	0.08	0.79	0.08	0.65	0.03	0.70	0.01
Cr_2O_3	0.09	34.9	0.02	0.01	0.03	0.01	0.01	0.00	0.01	0.00	0.01	0.00	0.02	0.00
FeO	2.46	2.73	3.88*	0.10	2.33	0.03	4.26*	0.08	2.27	0.03	3.26*	0.20	2.53	0.08
$\sum$	96.44		96.32	0.49	96.39	0.27	96.44	0.23	96.17	0.27	96.30	0.04	96.31	0.25
Na	0.234		0.178		0.155		0.178		0.151		0.123		0.443	
Mg	0.207		0.193		0.270		0.234		0.284		0.220		0.258	
^{T}Al	0.765		0.652		0.675		0.711		0.713		0.601		0.761	
^{M}Al	1.665		1.751		1.745		1.717		1.728		1.777		1.601	
Si	3.235		3.348		3.325		3.289		3.287		3.399		3.239	
K	0.724		0.289		0.357		0.307		0.407		0.231		0.573	
Ca	0.001		0.001		0.001		0.003		0.003		0.004		0.005	
Ti	0.027		0.031		0.033		0.037		0.038		0.031		0.034	
Cr	0.005		0.001		0.001		0.001		0.001		0.000		0.001	
Fe	0.135		0.206		0.123		0.227		0.121		0.172		0.139	
$\sum_T$	4.000		4.000		4.000		4.000		4.000		4.000		4.000	
$\sum_M$	2.040		2.183		2.173		2.215		2.172		2.200		2.033	
$\sum_I$	0.960		0.469		0.514		0.487		0.561		0.358		1.020	
$\sum_{All}$	7.000		6.652		6.687		6.702		6.733		6.558		7.053	

In WEDS mode, Na *Kα*, Mg *Kα*, Al *Kα*, Si *Kα*, K *Kα*, and Fe *Lα* were measured with WDS (*); all the other elements with EDS. (I), (II), and (III) represent the three different quantification procedures used. Reported compositions are the average of three spot analyses (SD, standard deviation). Upper columns: oxide Wt.%; lower columns: atoms per formula unit (a.p.f.u.) calculated on a base of 11 oxygens.
Σ_T = Si + ^{IV}Al; $\sum_M$ = Mg + ^{VI}Al + Ti + Cr + Fe; $\sum_I$ = Na + K + Ca; $\sum_{All}$ = sum of all cations.

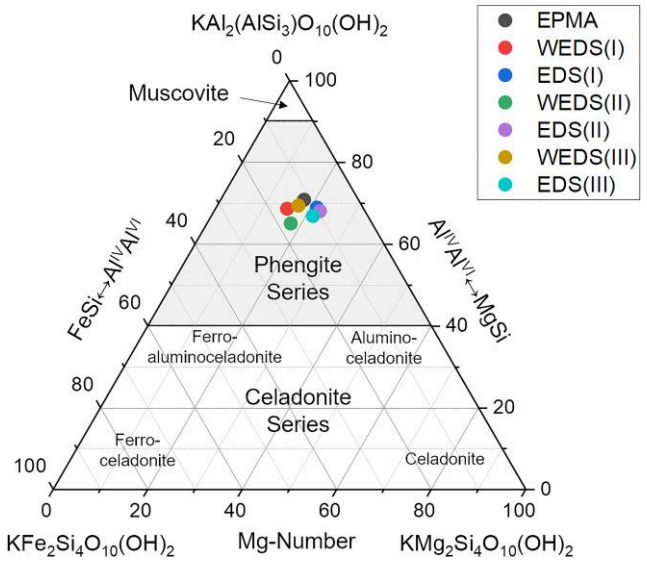

Fig. 10. Ternary plot showing the phengite compositions quantified by EPMA, WEDS, and EDS systems. WEDS and EDS analyses are distinguished according to the quantification procedure used (from Tappert et al., 2013, modified).

(II), phyllosilicate standards were used whenever possible. Thus, the following standards were employed: biotite (Mg, Al, Si, Ca, K, Ti, Mn, Fe), chlorite (Cr), and albite (Na). White mica was identified as phengite on the basis of EPMA analysis. Compositionally, phengite can be distinguished from muscovite by a higher Si, Fe, and Mg content and a lower Al content. Rieder et al. (1998) defined the phengite series as the potassic dioctahedral micas that fall compositionally between the joins of muscovite–aluminoceladonite and muscovite–celadonite. Tappert et al. (2013) devised a ternary diagram with vertices: muscovite, $[K(Al_2)AlSi_3O_{10}(OH)_2]_2$, and two hypothetical end members, $[KFe_2Si_4O_{10}(OH)_2]_2$ and $[KMg_2Si_4O_{10}(OH)_2]_2$. This ternary diagram is used to represent the microprobe analyses obtained in the present study (Fig. 10). As it can be seen from Table 6 and Figure 10, WEDS and EDS, disregarding the procedure used, slightly overestimate the Si content in comparison with EPMA. Moreover, WEDS yields a Fe/Mg ratio slightly higher than EDS. Sodium and especially K are underestimated irrespective of the procedure used, but when using procedure EDS(III). A possible explanation for the observed deviation is that Na and K, being monovalent cations with large ionic radii, are poorly bound to the mica interlayer and diffuse under the highly focused FEG beam. Indeed, procedure (III) was settled to minimize the migration of these monovalent cations establishing for it an *ad hoc* standardization and analysis protocol with a defocused beam [the following standards were used: biotite (Al, Si, Ca, K, Mg, Ti, Fe, Mn), chlorite (Cr), and albite (Na)]. However, as inferable from Table 6, this procedure only partially reduced the migration of interlayer cations, because the electron dose per atom, although reduced in procedure (III), is still larger than in EPMA, which uses a 5 μm beam size. The EDS(III) results are those that better mitigate migration. In the first instance, the explanation is similar to that reported above for the migration observed in the albite standard. In WEDS mode, EDS spectra are collected in 60 s, whereas WDS measures each element in sequence and a single analysis can last up to 6–8 min. Therefore, the electron dose received by the sample after measuring K and Na, especially if K and Na are not set at the beginning of the measuring sequence,

in WDS is much higher than the dose received after EDS measurement. The fact that migration effects are more evident for K than for Na could be explained by the larger ionic radius of $^{IX}K^{+}$ (1.55 Å) in comparison to $^{IX}Na^{+}$ (1.24 Å) and therefore the consequent lower bond strength and higher tendency to migrate of K. Our TDI tests actually reveal that the migration of Na in albite is more pronounced that the migration of K in biotite (Supplementary Figs. S1 and S2 and Tables S2 and S3 in the Supplementary Material). Along the same, Nielsen and Sigurdsson (1981) and Morgan and London (2005) found a higher mobility of Na in comparison to K in natural and synthetic glasses. These reverse aptitudes may be related to the different matrices (feldspar, mica, and glass) compared.

Concluding Remarks

- The most striking result of this investigation is that EPMA, *lato sensu*, i.e., either with WDS or EDS spectrometry, suffers from uncorrected matrix effects and is very sensitive to the standards used. That is a subject of a long-standing discussion in the EPMA community, which usually aligns to two opposite positions: (i) use of a pure element (or oxide, boride, etc.) or (ii) the use of a compound similar to the unknown material (Llovet et al., 2021 and references therein). In the first case, the composition is probably more accurately known, but a potentially larger matrix correction is required. In the second case, a smaller matrix correction is required, but there is less certainty in the standard's precise composition and homogeneity. This study confirms that the choice of the standards may affect the results. The involved differences may be such that the determined chemical composition may shift within or toward a nearby classification field, as it has been observed, for instance, for pyroxenes and amphiboles, respectively. Our feeling is that choosing standards with composition (and structure?) as close as possible to that of the investigated material may lead to more reliable results.
- Another prominent result is that element migration may be a serious problem, especially when monovalent, large ionic radius elements such as K and Na are present in the analyte. This problem is much more evident with FEG source systems than with conventional tungsten filament source systems, because of the much higher electron dose per atom of the former. The problem is more evident with WDS systems than with EDS systems, because of the longer acquisition time of the former. Moreover, it is more pronounced with parallel beam WDS instruments than with EPMA. Indeed, the presence of multiple spectrometers in the latter allows a reduction of the acquisition time per spot analysis and therefore a lower electron dose per atom. However, as demonstrated by TDI tests, alkali migration occurs in the first seconds of acquisition and the defocused beam selected in the present experiments, while preserving the spatial resolution required for a microprobe, was insufficient to eliminate alkali migration. Therefore, a possible route to eliminate this effect is the adoption of an *ad hoc* standardization and analysis protocol for sensitive materials, using a defocused beam size determined after TDI tests, ceding to spatial resolution if necessary, and perhaps considering TDI correction (McCubbin, et al., 2010; Donovan, et al., 2021; 2024; Llovet, et al., 2021).
- The analyses obtained with standard-based EDS, WEDS, and EPMA, although with significant differences in some cases, all make sense from a crystal chemistry point of view. In the discussion above, and generally in the relevant geological literature, it is assumed that EPMA analysis is basically correct and taken as reference. However, some of the problems disclosed in this study, such as uncorrected matrix effects and element migration, may affect EPMA as well, and it is not taken for granted that EPMA yielded more accurate results. Of course, EPMA, i.e., a dedicated instrument with up to five spectrometers concurrently acquiring data, has a head start. However, an integrated WEDS system achievable with a budget about five times smaller may be a viable cheaper solution whenever a SEM instrument is already present in-house. In this case, for routine analyses, as many elements as possible could be quantified using EDS and WDS could be used for elements with strongly interfering X-rays or with minor or trace concentrations (e.g., Goemann, 2018).
- The evaluation of the standardization results reveals that the combined WDS/EDS system releases consistent results. However, at least for the common minerals taken into consideration in this investigation, no obvious advantage of WEDS over EDS has emerged. Rather, while releasing comparable results in terms of accuracy and reproducibility, EDS, since collecting all elements at once and employing a lower beam current, has the advantage over WEDS of being faster and less damaging of minerals' integrity. More demanding mineral matrices, such as REE-bearing and light-element bearing minerals, such as B- or Be-bearing minerals in which parallel beam WDS would have, in principle, a strong advantage over EDS and Rowland circle WDS, are under investigation. Overall, although not examined here, the advantages of a WDS system over an EDS one remain undisputable in terms of (i) spectral resolution (in some cases compensated in EDS by deconvolution); (ii) trace element performance (lower limit of detection) due to higher P/B ratios (restricted for parallel beam WDS by upper energy limit); and (iii) light element sensitivity (only for parallel beam WDS).

Availability of Data and Materials

The authors have declared that no datasets apply for this piece.

Supplementary Material

To view supplementary material for this article, please visit https://doi.org/10.1093/mam/ozaf101.

Acknowledgments

The authors are grateful to Tiziano Catelani, Luca Pellegrino, and Fabrizio Vergani for preliminary tests on the parallel beam WDS. Ralf Terborg is greatly acknowledged for his help with the quantification/error calculation. We sincerely thank two anonymous reviewers for their very thorough and qualified review work.

Financial Support

The Platform of Microscopy of the University of Milano-Bicocca has been cofounded by the Italian Ministry of

University and Research (MIUR) through the "Dipartimenti di Eccellenza—2019" grant. The current study hasn't received any fund from any organizations or institutions.

Conflict of Interest

The authors declare that they have no competing interest.

References

Arrigoni F, Fumagalli P, Zanchetta S & Guastoni A (2020). Melt-rock interaction between granitic pegmatites and hosting amphibolites from the Chiavenna ophiolitic unit (tanno pegmatite field, Central Alps, North Italy). *Ofioliti* **45**, 13–23. https://doi.org/10.4454/ofioliti.v45i1.530

Buse B & Kearns S (2018). Quantification of olivine using Fe L α in electron probe microanalysis (EPMA). *Microsc Microanal* **24**, 1–7. https://doi.org/10.1017/S1431927618000041

Deer WA, Howie RA & Zussman J (2013). *An Introduction to the Rock-Forming Minerals*, 3rd Edition. Stevenage, Hertfordshire, UK: Mineralogical Society of Great Britain and Ireland.

Donovan JJ, Allaz JM, Von Der Handt A, Seward GGE, Neill O, Goemann K, Chouinard J & Carpenter PK (2021). Quantitative WDS compositional mapping using the electron microprobe. *Am Mineral* **106**, 1717–1735. https://doi.org/10.2138/am-2021-7739

Donovan J, Moy A & Von Der Handt A (2024). Software methods and tools for WDS light element analysis. *Microsc Microanal* **30**, ozae044.087. https://doi.org/10.1093/mam/ozae044.087

Droop GTR (1987). A general equation for estimating Fe^{3+} concentrations in ferromagnesian silicates and oxides from microprobe analyses, using stoichiometric criteria. *Mineral Mag* **51**, 431–435. https://doi.org/10.1180/minmag.1987.051.361.10

Drouin D, Couture AR, Joly D, Tastet X, Aimez V & Gauvin R (2007). CASINO V2.42 - A fast and easy-to-use modeling tool for scanning electron microscopy and microanalysis users. *Scanning* **29**, 92–101. https://doi.org/10.1002/sca.20000

Goemann K (2018). Comparison and combination of energy and wavelength dispersive X-ray spectrometry in electron probe microanalysis of minerals and glasses. *Microsc Microanal* **24**, 748–749. https://doi.org/10.1017/S1431927618004233

Gopon PN (2016). Electron probe sub-micron analysis in geoscience: Problems and potential solutions of low voltage electron microprobe analysis, as applied to reduced lunar phases and pyroxene lamellae (Order No. 10154796). Available from Natural Science Collection; ProQuest Dissertations & Theses Global. (1817382984). Retrieved from https://www.proquest.com/dissertations-theses/electron-probe-sub-micron-analysis-geoscience/docview/1817382984/se-2

Grew ES, Locock AJ, Mills SJ, Galuskina IO, Galuskin EV & Halenius U (2013). Nomenclature of the garnet supergroup. *Am Mineral* **98**, 785–811. https://doi.org/10.2138/am.2013.4201

Hawthorne FC, Oberti R, Harlow GE, Maresch WV, Martin RF, Schumacher JC & Welch MD (2012). Nomenclature of the amphibole supergroup. *Am Mineral* **97**, 2031–2048. https://doi.org/10.2138/am.2012.4276

Larionov YV (2014). Measurement of the SEM-beam diameter using a relief structure: Influence of contamination. *J Synch Investig* **8**, 1137–1145. https://doi.org/10.1134/s1027451014050127

Leake BE, Woolley AR, Arps CES, Birch WD, Gilbert MC, Grice JD, Hawthorne FC, Kato A, Kisch HJ, Krivovichev VG, Linthout K, Laird J, Mandarino J, Maresch WV, Nickel EH, Rock NMS, Schumacher JC, Smith DC, Stephenson NCN, Ungaretti L, Whittaker EJW & Youzhi G (1997). Nomenclature of amphiboles. Report of the subcommittee on amphiboles of the international mineralogical association, commission on new minerals and mineral names. *Mineral Mag* **61**, 295–321. https://doi.org/10.1127/ejm/9/3/0623

Llovet X, Moy A, Pinard PT & Fournelle JH (2021). Electron probe microanalysis: A review of recent developments and applications in materials science and engineering. *Prog Mater Sci* **120**, 100818. https://doi.org/10.1016/j.pmatsci.2021.100818

McCubbin FM, Steele A, Nekvasil H, Schnieders A, Rose T, Fries M, Carpenter PK & Jolliff BL (2010). Detection of structurally bound hydroxyl in fluorapatite from Apollo mare basalt 15058,128 using TOF-SIMS. *Am Mineral* **95**, 1141–1150. https://doi.org/10.2138/am.2010.3448

Morgan GB & London D (1996). Optimizing the electron microprobe analysis of hydrous alkali aluminosilicate glasses. *Am Mineral* **81**, 1176–1185. https://doi.org/10.2138/am-1996-9-1016

Morgan GB & London D (2005). Effect of current density on the electron microprobe analysis of alkali aluminosilicate glasses. *Am Mineral* **90**, 1131–1138. https://doi.org/10.2138/am.2005.1769

Morimoto N (1988). Nomenclature of pyroxenes. *Mineral Petrol* **39**, 55–76. https://doi.org/10.1007/BF01226262

Moy A, Fournelle JH & Von Der Handt A (2019). Solving the iron quantification problem in low-kV EPMA: An essential step toward improved analytical spatial resolution in electron probe microanalysis—Olivines. *Am Mineral* **104**, 1131–1142. https://doi.org/10.2138/am-2019-6865

Moy A, Von Der Handt A & Fournelle J (2022). Solving the iron quantification problem in low-kV EPMA: An essential step toward improved analytical spatial resolution in electron probe microanalysis—Fe-sulfides. *Am Mineral* **107**, 1532–1544. https://doi.org/10.2138/am-2022-8027

Newbury DE & Ritchie NWM (2015). Performing elemental microanalysis with high accuracy and high precision by scanning electron microscopy/silicon drift detector energy-dispersive X-ray spectrometry (SEM/SDD-EDS). *J Mater Sci* **50**, 493–518. https://doi.org/10.1007/s10853-014-8685-2

Newbury DE & Ritchie NWM (2019). Electron-excited X-ray microanalysis by energy dispersive spectrometry at 50: Analytical accuracy, precision, trace sensitivity and quantitative compositional mapping. *Microsc Microanal* **25**, 1075–1105. https://doi.org/10.1017/S143192761901482X

Nielsen CH & Sigurdsson H (1981). Quantitative methods for electron microprobe analysis of sodium in natural and synthetic glasses. *Am Mineral* **66**, 547–552. https://api.semanticscholar.org/CorpusID:40201692

Pleuger J, Hundenborn R, Kremer K, Babinka S, Kurz W, Jansen E & Froitzheim N (2003). Structural evolution of Adula nappe, Misox zone, and Tambo nappe in the San Bernardino area: Constraints for the exhumation of the adula eclogites. *Mitteilungen der Österreichischen Geologischen Gesellschaft* **94**, 99–122. https://ajes.at/index.php/archive/mitteilungen-der-oegg#95-band-94

Pouchou JL & Pichoir F (1991). Quantitative analysis of homogeneous or stratified microvolumes applying the model "PAP". In *Electron Probe Quantitation*, Heinrich KFJ, Newbury DE (Eds.), pp. 31–75. Boston, MA: Springer.

Reed SJ (2010). *Electron Microprobe Analysis and Scanning Electron Microscopy in Geology*, 2nd edition. UK: Cambridge University Press.

Rieder M, Cavazzini G, D'Yakonov YS, Frank-Kamenetskii VA, Gottardi G, Guggenheim S, Koval PV, Müller G, Neiva AMR, Radoslovich EW, Robert JL, Sassi FP, Takeda H, Weiss Z & Wones DR (1998). Nomenclature of the micas. *Can Mineral* **36**, 905–912. https://doi.org/10.1346/ccmn.1998.0460513

Seddio SM (2019). A comparative evaluation of the intensities, spectral resolution, and overall time of acquisition achievable by SEM-based parallel beam WDS and SEM-based Rowland circle WDS. *Microsc Microanal* **25**, 836–837. https://doi.org/10.1017/S1431927619004914

Smith JV (1974). Nomenclature and general properties of feldspars. In *Feldspar Minerals*, Smith JV (Ed.), pp. 415–460. Heidelberg, Berlin, Germany: Springer.

Tappert MC, Rivard B, Giles D, Tappert R & Mauger A (2013). The mineral chemistry, near-infrared, and mid-infrared reflectance spectroscopy of phengite from the Olympic dam IOCG deposit, South Australia. *Ore Geol Rev* **53**, 26–38. https://doi.org/10.1016/j.oregeorev.2012.12.006